Trabajo de Fin de Grado

GRADO EN FÍSICA

Dark Matter as Bose–Einstein Condensates

José Miguel Martín Pérez

Dirigido por:

Dr. Vicente Delgado Borges

Universidad de La Laguna

Septiembre 2020

Contents

Resumen

La materia oscura es uno de los problemas más importantes y actuales de la física. Por lo general, se considera constituida por partículas clásicas moviéndose a velocidades no relativistas y que solo interaccionan gravitatoriamente. Este es el que se conoce como modelo de materia oscura fría (CDM). A pesar de ser el modelo más extendido, las simulaciones bajo su marco teórico presentan serios problemas. En este trabajo estudiamos un modelo alternativo para la materia oscura, que consiste en suponerla compuesta por partículas cuánticas ultraligeras agregadas en condensados de Bose–Einstein.

Al final del trabajo se comparan ambos modelos con los datos experimentales y se dan unas nociones de hacia dónde se dirige la investigación actualmente en este campo.

1 Introduction

The discovery of both dark matter and dark energy is one of the most important scientific events in recent times. Together, they constitute the 95% of the Universe. The rest, a 5%, is the conventional matter. But dark matter and energy not only are important by their abundance but also because they are different and we hope that with a precise description we will be able to understand new and deeper aspects about the universe.

According to the last estimations, dark matter represents a 27% of the total content of the universe, being therefore five or six times more abundant than ordinary matter. The concept of dark matter was introduced as a solution to the dissonance that exits between the observational orbits of the stars in their galaxies and the theoretical predictions. This problem, that will be explained deeper in the first section, basically can be stated as follows: Theoretically, the velocity of the stars far away from the centre of their galaxies, where there are almost no stars and there are little contributions to the total mass of the galaxies, should decrease rapidly with the distance; however, observations indicate that this is not the case and the stars actually maintain their velocities almost constant. To explain this fact the existence of invisible matter was proposed. This must be matter that interacts only gravitationally with the ordinary matter and was called dark matter (DM).

Apart from the hypothesis of the existence of this new type of matter, other solutions were also proposed. The most important consists in modified theories of gravity, which suppose that the disagreement between theory and observations is due to a failure of the Newtonian gravity theory at large distances (galactic scales). These are the MOND theories (Modified Newtonian Dynamics).

The reason to put more emphasis on the dark matter hypothesis is that there are a series of evidences that support its existence. We will also mention these evidences in the first section.

Nowadays, the most accepted cosmological model is the ΛCDM model, where Λ denotes the dark energy and CDM means cold dark matter. In contrast to the hot dark matter model, the CDM model assumes that dark matter particles move at low velocities, i.e., at non-relativistic velocities. In the cold dark matter theory, the structure grows hierarchically, with small objects collapsing under their self-gravity first and merging in a continuous hierarchy to form larger and more massive objects (bottom-up).

The viability of the ΛCDM conception was first evaluated using computational simulations. The behaviour of the dark matter can be simulated in computers chunking a portion of the universe and evolving it (N-body simulations). Since the particles interact only through gravity, these simulations are called collisionless simulations. Predictions of the cold dark matter paradigm agree in general with observations of cosmological large-scale structure.

On the other hand, since the 1990's the simulations became sufficiently powerful to make detailed predictions of the internal structure of halos in different cosmological scenarios. These simulations highlighted the universal nature of the DM halos, formed by means of

collisionless collapse. In addition, these simulations predicted that the matter density of halos satisfies the Navarro–Frenk–White (NFW) profile,

$$\rho_{NFW}(r) = \frac{\rho_s}{(r/r_s)(1 + r/r_s)^2}, \tag{1}$$

where r_s is a scale radius and ρ_s is a characteristic density.

However, these powerful simulations started to point out a certain number of deficiencies in the CDM scenarios. The most obvious was the overabundance, by more than an order of magnitude, of small dark matter halos compared to the number of small dwarf galaxies observed orbiting the Milky Way or others galaxies ("the missing satellites problem"). Worse, the simulations significantly overpredicted the density of DM at the centre of galaxies. This can be observed in the NFW density profile, which predicts a well pronounced central cusp. On the observational side, high-resolution rotation curves show that the actual distribution of dark matter is much shallower than this and that it presents a nearly constant density core. This discrepancy between the CDM model and observations is called "the cusp-core problem".

The differences between observations and simulations in the framework of the ΛCDM model are particularly important in the case of the recent observations of the dwarf galaxies done by "The HI Nearby Galaxy Survey" (THINGS) [1]. Dwarf galaxies are cosmic structures dominated by dark matter with a very small contribution of baryonic matter to the total matter content. The observed rotation curves are better described by core-like models instead of cusp-like models.

The CDM model is being challenged by these problems. In response to the apparent inability of this model to solve the above problems, new models for the dark matter have been proposed. One of them, the one we are interested in, models DM as a Bose–Einstein condensate. Its more recent results are promising.

The aim of this work is to study the main theoretical aspects of this model. The structure of the work consists of a first section explaining why the idea of the dark matter emerges and the evidences of its existence, followed by two sections about Bose–Einstein condensates —one dedicated to a conceptual introduction and the other dedicated to the derivation of the equation describing the dynamical evolution of the condensates (the Gross–Pitaevskii equation). Then, there are three sections dedicated to the derivation of the density profiles of the dark matter halos considered as Bose–Einstein condensates. Finally, the last two sections present the results of this model and the conclusions.

2 Dark matter: necessity and evidences

En esta sección se hace una revisión histórica de los motivos que llevaron a proponer la existencia de materia oscura en el universo y se dan una serie de pruebas para defender la hipótesis de la materia oscura frente a otras hipótesis, como las teorías MOND.

2.1 Rotation curves

To understand the original proposal of the existence of dark matter we need to first introduce a very simple but important formula of classical dynamics. Astronomical objects moving in circular orbits of radius r around a mass $M(r)$ have only centripetal acceleration and, as a consequence, their velocities satisfy

$$v = \sqrt{\frac{G\,M(r)}{r}}. \tag{2}$$

This equation can be used to determine the mass of astronomical objects by simply measuring the velocity of the bodies orbiting them. The use of Eq. (2) allowed revealing the existence of the dark matter for the first time.

In principle, Eq. (2) is only strictly valid for circular orbits. However, it is also satisfied in average in the case of elliptical orbits. Thus, if we measure the velocity of many bodies orbiting around a large mass, we can use Eq. (2) to determine the value of this mass.

Considering in a galaxy the velocity of stars with different distances to the galactic centre we can determine the amount of mass bounded by the orbit of each star, that is the effective mass that attracts it. In this way it is possible to know the mass distribution in the galaxy. This was the work developed in the 1960's by Vera Rubin and Kent Ford [2].

A reasonable expectation about the mass of the galaxies already existed. In theory, the mass of the galaxies came mainly from stars and galaxy gases. The stellar mass could be measured using the galaxy brightness and nowadays the mass that galactic gas contains is known thanks to the X-ray spectrum that it emits. All this matter constitutes the major part of the ordinary mass of the galaxy, the only one known in Rubin times. Therefore, it existed a clear idea about the galaxy mass and its distribution.

Concretely, at a large distance from the centre there are barely any stars and gas that contributes to the galactic mass and this would cause the velocity of stars far away from the galactic centre to decrease rapidly with distance. However, these were not the results that Rubin and Ford found: the star velocities remained constant even for large radii r.

The easiest explanation to this observation is that apart from visible matter, invisible matter (dark matter) exists, which extends much further than the apparent bounds of the galaxies and contains more mass than the visible matter. Thus, an increase in r is compensated by other in $M(r)$, remaining the velocity of distant stars constant.

Rubin and Ford studied more than 60 galaxies, finding the same phenomenon. The conclusions of this study have being confirmed later by other independent observations. Typically the ordinary mass of a galaxy is in the order of the 10% of the total, being the remaining 90% dark matter. However, at cosmic level the proportions are 80–85% of dark matter and 15–20% of ordinary matter. The reason is that the majority of the ordinary matter is in the intergalactic gas.

In general, the study of Rubin and Ford is considered as the first clear evidence of the presence of dark matter. Nevertheless, Fritz Zwicky was the first astronomer who proposed

the existence of dark matter based on an observational evidence in 1933 [2]. Zwicky studied the Coma Cluster, that contains over 1000 identified galaxies, and observed that the velocities of the galaxies were much higher than expected. Zwicky attributed this to a "dark matter" in the cluster, although he overestimated its amount because he did not consider the intergalactic gas due to the fact that he did not have the needed instruments.

Anyway, it was not clear, even after the Rubin–Ford study, whether the dark matter was only ordinary matter difficult to detect or a new unknown type of matter. The possibility that the Newton law failed at large distances also existed, in which case one could not use Eq. (2) to infer the matter content of the galaxies.

2.2 Cosmic experiments

The question that immediately arises is whether on galactic scales the Newton's law remains valid. In the previous subsection we used repeatedly Eq. (2). In that relation we assume that G is a constant but it is possible that, for example, at large distances G were proportional to r. Thus, an increase in the denominator would be compensated by an increase of G in the numerator. In this way, it would not be necessary to impose the existence of dark matter to explain anomalous velocities at large distances. This type of theories constitute the MOND theories.

One can think that the problem we are dealing with could be resolved using the theory of general relativity since it is a modification of the gravitation laws. We will develop this idea a little in what follows.

For the case of a large central mass M we can deduce, using general relativity theory, a very similar equation to the Newton's law of universal gravitation with little modifications:

$$F = G\frac{Mm}{r^2} + f, \tag{3}$$

where f is an addition of terms that depend only on the distance r and the velocity of the two masses that attract each other. The most important term is

$$f = -\frac{4}{c^2}\frac{G^2M^2m}{r^3} + ... \tag{4}$$

In general f is a very small quantity but it is always there. It is the cause of the apsidal precession, which is notable in Mercury for example. Since this term is inversely proportional to r^3, the value of f is relatively more important when the distance is smaller. Hence, due to the fact that we are dealing with huge star orbits, relativistic effects are absolutely negligible.

Another important effect of general relativity is the light deflection. This effect is so known that we can use it as an alternative method to determine the mass of an astronomical object by measuring how the light rays are curved. The experiments with gravitational lenses have confirmed that dark matter is five or six times more abundant than the ordinary

one, in perfect accordance with the estimations of the orbits method. But they have also provided an impressive evidence that dark matter is really there...

The hierarchy of mass in a cluster is given by a major part of dark matter and a rest of ordinary mass, mainly intergalactic gas and, in much lower amount, individual galaxies. This gas can be observed by means of X-ray emission, which allows us know its temperature, abundance and mass.

MOND theories claim that dark matter does not exist. If this were correct the major part of the cluster mass would be in the intergalactic gas and then it would be the main responsible of the gravitational lensing effect that the cluster has.

Figure 1: As can be appreciated in the picture, the gas clouds (pink) have been separated from the individual galaxies and the dark matter (blue). Source: NASA / Chandra X-Ray Observatory (*https://chandra.harvard.edu/photo/2006/1e0657/more.html*).

Figure 1 shows the Bullet Cluster, where actually there are two clusters that have being colliding for hundreds of millions of years. In this collision the intergalactic gas (which appears in the centre of the picture in pink colour) has been separated from the individual galaxies residing within the dark matter halos (represented in blue colour). The explanation is that while both gas clouds interact and slow down, the galaxies and dark matter cross with almost no interaction since they are only subject to gravitational forces.

We then have to consider the gravitational lensing effect produced by the cluster. The clear bluish spots in Fig. 1 represent the places where the effect of gravitational lensing is higher and, therefore, where the major part of matter is. Hence, we see that the major part of matter is not in the gas clouds, so MOND hypothesis does not sustain itself because if there were no dark matter, the clear spots would be on the gas clouds.

The Bullet Cluster is considered to be the most direct and impressive evidence of the

existence of the dark matter. Moreover, it offers us new data. Concretely, it indicates that aside its little interaction with ordinary matter it also interacts weakly with itself. Otherwise, the dark matter clouds would also have rubbed each other across and lagged behind. After these observations, other clusters collisions have been analysed.

Another interesting fact against MOND theories is that the percentage of dark matter varies from one galaxy to another despite that the amount of conventional mass is similar. This is something that MOND theories do not expect.

2.3 Nucleosynthesis

According to the Big Bang theory, when the universe was about 100 seconds old its temperature was a thousand of millions of kelvin. With this temperature, protons, neutrons and electrons were free. But just at that moment, the conditions provoked the nucleosynthesis, and protons and neutrons blended to form simple nuclei such as deuterium or helium. The theoretical amounts of deuterium, helium-3 and lithium are given by calculations that use relativity equations and knowledge about nuclear processes. The crucial point is that to do these calculations the ordinary matter density of the universe is also necessary, which is extracted from the observations of the galaxies and the intergalactic gas. The obtained amounts are in good agreement with the abundances that we measure currently. This tells us that dark matter, which is six times more abundant, cannot be baryonic matter we have not detected.

2.4 Anisotropies of the CMB

After nucleosynthesis, we had a universe with simple nuclei and other charged particles, that is, a plasma. These particles interacted widely with photons, which is the reason they were trapped. However, when the universe grew cooler and the photons decreased their energy, nuclei and electrons could combine to form neutral atoms (recombination) that interacted to a lesser degree with photons. The atoms could not scatter the thermal radiation and photons started to travel freely through the space. Due to the universe expansion, the wavelength of these photons grew, decreasing in turn their energy and converting into microwaves. Thus, we have a Cosmic Microwave Background (CMB) radiation that is detected in all directions.

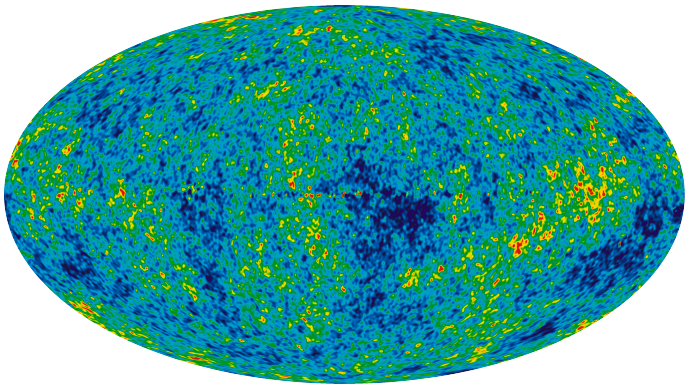

Figure 2: Map that highlights the anisotropies of the temperature of the CMB radiation. The colour of each point represents the energy of each photon: the hottest are represented in red and the coldest in dark blue. Source: NASA / WMAP Science Team (*https://wmap.gsfc.nasa.gov/media/101080*).

The CMB, that in principle is homogeneous, actually presents small fluctuations detected for the first time by the satellite COBE. These anisotropies are on the order of one part per million and point small differences in the temperatures of photons that come from different places of the sky. In a plasma, hotter zones are denser zones too. In this way, we can interpret Fig. 2 as a map of densities of the primordial universe.

The origin of the oscillations of density are the pressure waves that crossed the space. As can be inferred from the irregularity of Fig. 2, the universe was populated by pressure waves of different wavelengths: the dominant or fundamental tone and the harmonics. Using a mathematical analysis of the map one can find the acoustic spectrum of the universe. This is what Fig. 3 represents. It shows several peaks corresponding to the dominant pressure waves at the moment of the recombination.

Although the gravitational action of baryons makes them tend to collapse in dense halos, the photon pressure tends to eliminate the created anisotropies. These two effects compete and with this confrontation the pressure waves appear.

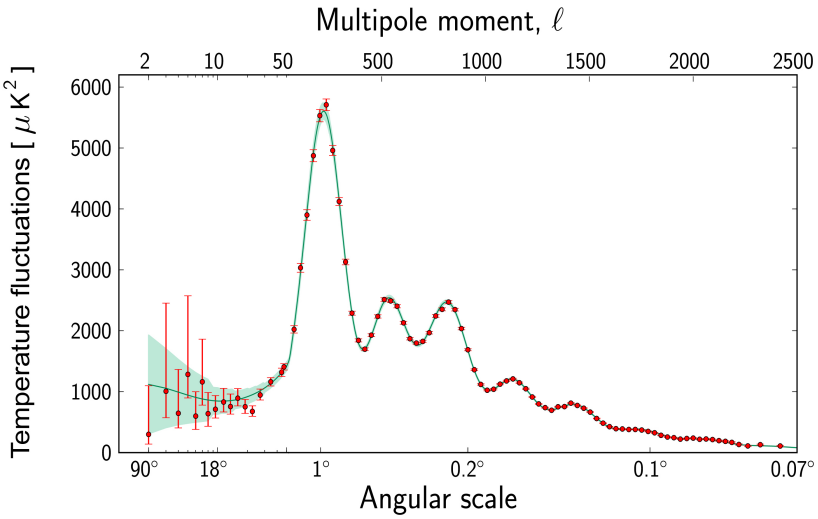

Figure 3: Acoustic spectrum of the universe in the recombination epoch. The points represent the observations with its errorbars and the solid curve represents the theoretical prediction. Source: ESA and the Planck Collaboration (*https://sci.esa.int/s/wRVmdjw*).

One can extract important information from the peak structure about the proportions of matter in the universe. The height of the first peak (the fundamental) is related with the density of the total matter. What is obtained is a 32% of the critical density, fact that is also found from current observations of the density of the dark and ordinary matter. The second peak is related to the radiation pressure of the plasma and, therefore, only with ordinary matter. From this peak what is obtained is a density of 5% of the critical density, which reinforces our data again.

3 Bose–Einstein condensates

En esta sección se hace una introducción tanto histórica como conceptual de los condensados de Bose–Einstein.

All particles can be classified into two types based on their spin: bosons, with integer spin, and fermions, with half-odd-integer spin. According to the symmetrization postulate of quantum mechanics, the wave functions that describe a system of bosons must be symmetric under interchange of any two particles, in contrast to fermions wave functions, which must be antisymmetric under this interchange. But the aspect of bosons that interests us the most is that, unlike fermions, they do not have to fulfill the Pauli exclusion principle. In this way, bosons may occupy the same single-particle state forming a so-called Bose–Einstein condensate, which can be interpreted as a new state of matter.

We can estimate the order of magnitude of the transition temperature to the Bose–Einstein condensed state from dimensional arguments. For a uniform gas of particles, the relevant quantities are the particle mass m, the particle density n and the Planck constant $h = 2\pi\hbar$. The only magnitude with energy dimensions that we can construct with them is $\hbar^2 n^{2/3}/m$. On the other hand, the thermal energy is proportional to $k_B T_c$, where k_B is the Boltzmann constant and T_c is the condensation temperature. Dividing both energies we obtain an adimensional numerical factor C. Isolating T_c:

$$T_c = C\frac{\hbar^2 n^{2/3}}{m k_B}. \tag{5}$$

C is approximately equal to 3.3 [3]. Substituting in (5) as an example the mass and density of liquid ^{4}He at saturated vapour pressure one obtains a condensation temperature of approximately 3.13 K.

Another equivalent way of obtaining the transition temperature is by means of the comparison between the thermal de Broglie wavelength λ_T and the average distances among particles. In a non-relativistic context the wavelength of a particle of mass m is related to the magnitude of the lineal momentum p by

$$\lambda_T = \frac{h}{p}\,. \tag{6}$$

Substituting p in terms of the kinetic energy $E_K = p^2/2m$:

$$\lambda_T = \frac{h}{\sqrt{2mE_K}}\,. \tag{7}$$

Since in the quantum case the average kinetic energy of free particles is $E_K = \pi k_B T$, we arrive at

$$\lambda_T = \sqrt{\frac{h^2}{2\pi m k_B T}} = \sqrt{\frac{2\pi\hbar^2}{m k_B T}}\,. \tag{8}$$

On the other hand, we can obtain the average distance among particles inside a volume V as $(V/N)^{1/3} = n^{-1/3}$. Statistical Physics considers that quantum effects are relevant when the de Broglie wavelengths of the particles are equal or greater than the average distances among them, i.e. when

$$\lambda_T = \sqrt{\frac{2\pi\hbar^2}{m k_B T}} \geq n^{-1/3}. \tag{9}$$

In the opposite case, the physics of the system can be described in classical terms. Bose–Einstein condensation (BEC) sets in when the temperature is so low that λ_T becomes comparable to $n^{-1/3}$.

3.1 Bose–Einstein condensates in experiments

Bose–Einstein condensates (BECs) were obtained for the first time in a series of experiments with rubidium and sodium vapours, in which the atoms were trapped with magnetic fields and cooled down to temperatures on the order of fractions of microkelvins. Once the atoms were left free switching off the confinement trap, pictures were taken with optic methods. A sharp peak in the velocity distribution of the atoms, that is a clear signature of BEC, was observed below a certain critical temperature. In the same year, signatures of BEC were also found in lithium vapours [4].

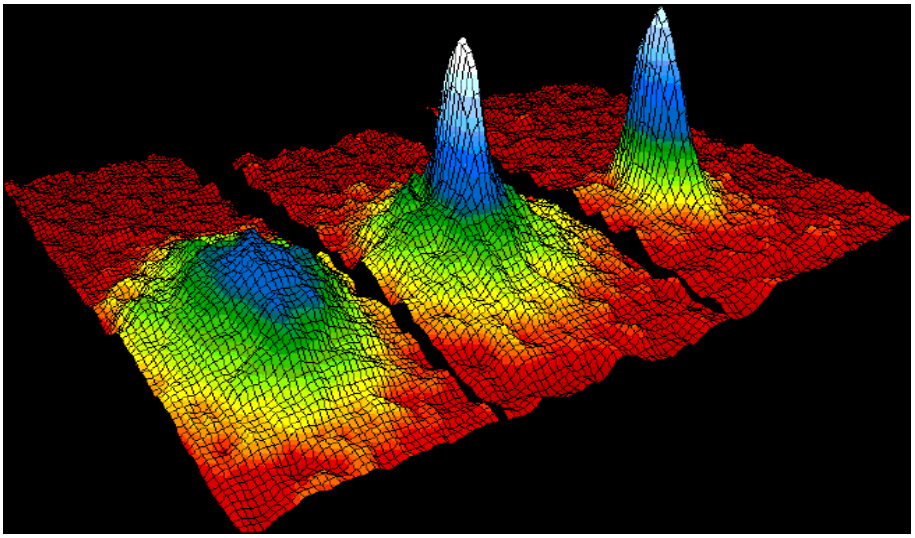

Figure 4: "Images of the velocity distribution of rubidium atoms in the experiment by Anderson et al. (1995), taken by means of the expansion method. The left frame corresponds to a gas at a temperature just above condensation; the center frame, just after the appearance of the condensate; the right frame, after further evaporation leaves a sample of nearly pure condensate. The field of view is $200\,\mu$m $\times$ $270\,\mu$m, and corresponds to the distance the atoms have moved in about 1/20 s. The color corresponds to the number of atoms at each velocity, with red being the fewest and white being the most. From Cornell (1996)" Source: Ref. [4].

These experiments on the alkalis carried out in 1995 constituted a milestone in the history of the BEC. Nevertheless, they were not the first attempts to condense atomic gases. More than 15 years ago there was a series of experiments with hydrogen atoms, which were cooled in a dilution refrigerator, then inserted in a magnetic trap and finally cooled by evaporation. Although these experiments were close to obtaining the BEC they were still limited by recombination of atoms in molecules.

In the 1980's cooling and trapping techniques based on laser were developed, such as laser cooling and magneto-optical trapping. Alkali atoms adapt well to these methods because their optical transitions can be excited by available lasers and because their internal di-

agram of energy levels is favorable for cooling at very low temperatures. Once they are trapped, their temperature can be reduced even further by evaporation. Combining laser and evaporative cooling for alkali atoms, researchers finally reached the temperatures and densities required to observe condensates.

It is important to highlight that, in these conditions, the equilibrium configuration of the system would be the solid phase. Therefore, to observe a BEC we have to maintain the system in a metaestable gas phase for a relatively long time. As collisions among three bodies are rare events in cold and dilute gases, their useful lifetimes are sufficiently long for the experiments.

4 Derivation of the Gross–Pitaevskii equation

La ecuación de Gross–Pitaevskii es la ecuación que describe la dinámica de los condensados de Bose–Einstein. En esta sección la derivamos detalladamente a partir de la minimización del funcional de la energía.

The Gross–Pitaevskii equation (GPE) is the equation that describes the dynamics of Bose–Einstein condensates. In the two following subsections we make use of the quantum variational principle to derive in detail both the stationary and the time-dependent GPE.

We consider N identical bosons at a temperature $T = 0$ K under the action of a certain external potential $V_{ext}(\vec{r})$. Taking into account that bosons also interact among them, the hamiltonian H of the system can be written as follows:

$$H = \sum_{i=1}^{N} \left(\frac{\vec{p_i}^2}{2m} + V_{ext}(\vec{r}_i) \right) + \frac{1}{2} \sum_{i=1}^{N} \sum_{j \neq i} V(|\vec{r}_i - \vec{r}_j|) \equiv H_1 + H_{int} \,. \tag{10}$$

H_1 corresponds to the hamiltonian of the N particles in the external potential, with no interactions among them, while H_{int} accounts for two-body inter-particle interactions. In dilute BECs, three-body and higher-order interactions are negligible.

While at room temperature bosons occupy different levels of energy, at very low temperatures a large ratio of them condense at the same time in the lowest level of energy. In a *pure* BEC all the bosons concentrate in the same single-particle state (the fundamental state $|\phi\rangle$). Therefore, we can use the ansatz that the total wave function $|\psi\rangle$ of a BEC of N bosons can be written as the following symmetric product of single-particle fundamental states:

$$|\psi\rangle = |\phi(1)\rangle|\phi(2)\rangle...|\phi(N)\rangle. \tag{11}$$

In coordinate representation we have

$$\psi(\vec{r}_1, \vec{r}_2, ..., \vec{r}_N) = \prod_{i=1}^{N} \phi(\vec{r}_i). \tag{12}$$

4.1 Stationary equation

Within the subspace formed by all the product states $|\psi\rangle$ of the form (11), the state that gives the best approximation to the fundamental state of the global system is the one that minimises the quantity

$$E[\psi] = \frac{\langle\psi|H|\psi\rangle}{\langle\psi|\psi\rangle}, \tag{13}$$

where $E[\psi]$ is a functional of ψ, and therefore also of ϕ. In other words, a number $E[\phi]$ is associated with each function ϕ by the functional.

Physical states are stationary solutions of the energy functional, $\delta E[\psi] = 0$, satisfying the normalisation condition $\langle\psi|\psi\rangle = 1$, which using Eq. (11) can trivially be stated in function of $|\phi\rangle$ as $\langle\phi|\phi\rangle = 1$. Hence, the energy functional becomes $E = \langle\psi|H|\psi\rangle$ and the fundamental state we are searching for must obey simultaneously the following conditions:

$$\delta\langle\psi|H|\psi\rangle = 0, \tag{14}$$

$$\langle\phi|\phi\rangle = 1. \tag{15}$$

For convenience, we will divide the calculation of the energy functional $E[\phi]$ in two parts: $E_1 \equiv \langle\psi|H_1|\psi\rangle$ and $E_2 \equiv \langle\psi|H_{int}|\psi\rangle$.

$$E_1 = \langle\psi|H_1|\psi\rangle = \int d\vec{r}_1 d\vec{r}_2 ... d\vec{r}_N \sum_i \left[\psi^*(\vec{r}_1, ..., \vec{r}_N)\left(-\frac{\hbar^2}{2m}\nabla_i^2 + V_{ext}(\vec{r}_i)\right)\psi(\vec{r}_1, ..., \vec{r}_N)\right]$$

$$= \sum_i \int d\vec{r}_1 ... d\vec{r}_N \left[\phi^*(\vec{r}_1)...\phi^*(\vec{r}_N)\left(-\frac{\hbar^2}{2m}\nabla_i^2 + V_{ext}(\vec{r}_i)\right)\phi(\vec{r}_1)...\phi(\vec{r}_N)\right]. \tag{16}$$

Due to the fact that the operators only act on the i^{th} coordinates, the above equation reduces to

$$E_1 = \sum_i \left[\int d\vec{r}_1 |\phi(\vec{r}_1)|^2 ... \int d\vec{r}_i \phi^*(\vec{r}_i)\left(-\frac{\hbar^2}{2m}\nabla_i^2 + V_{ext}(\vec{r}_i)\right)\phi(\vec{r}_i) ... \int d\vec{r}_N |\phi(\vec{r}_N)|^2\right]$$

$$= \sum_i \int d\vec{r}_i \phi^*(\vec{r}_i)\left(-\frac{\hbar^2}{2m}\nabla_i^2 + V_{ext}(\vec{r}_i)\right)\phi(\vec{r}_i)\,, \tag{17}$$

where we have used the normalisation condition in the last step, $\langle\phi|\phi\rangle = \int d\vec{r}_k |\phi(\vec{r}_k)|^2 = 1$. Taking into account that all the terms in the sum are identical, we finally obtain

$$E_1 = \langle\psi|H_1|\psi\rangle = N \int d\vec{r}\phi^*(\vec{r})\left(-\frac{\hbar^2}{2m}\nabla^2 + V_{ext}(\vec{r})\right)\phi(\vec{r}). \tag{18}$$

As for the second contribution:

$$E_2 = \langle\psi|H_{int}|\psi\rangle = \frac{1}{2}\sum_i\sum_{j\neq i}\int d\vec{r}_1...d\vec{r}_N\phi^*(\vec{r}_1)...\phi^*(\vec{r}_N)V(|\vec{r}_i-\vec{r}_j|)\phi(\vec{r}_1)...\phi(\vec{r}_N)$$

$$= \frac{1}{2}\sum_i\sum_{j\neq i}\int d\vec{r}_i d\vec{r}_j\phi^*(\vec{r}_i)\phi^*(\vec{r}_j)V(|\vec{r}_i-\vec{r}_j|)\phi(\vec{r}_i)\phi(\vec{r}_j)\,. \tag{19}$$

In a dilute and cold gas only binary collisions at low energy are relevant. These collisions are characterised by a single parameter, independently of the details of the two-body potential. This allows us to replace $V(|\vec{r}_i-\vec{r}_j|)$ in Eq. (19) by an effective contact interaction

$$V(|\vec{r}_i-\vec{r}_j|) = \eta\delta(\vec{r}_i-\vec{r}_j), \tag{20}$$

where the coupling constant η is related with the s-wave scattering length a_s by means of

$$\eta = \frac{4\pi\hbar^2 a_s}{m}. \tag{21}$$

This enables us to carry out one of the two integrals in a trivial manner

$$E_2 = \frac{1}{2}\sum_i\sum_{j\neq i}\int d\vec{r}_i\phi^*(\vec{r}_i)\phi^*(\vec{r}_i)\eta\phi(\vec{r}_i)\phi(\vec{r}_i) = \frac{1}{2}\eta\sum_i\sum_{j\neq i}\int d\vec{r}_i|\phi(\vec{r}_i)|^4. \tag{22}$$

The sum over j can be readily performed taking into account that nothing depends on j and that, as j may not be equal to i, there will be $N-1$ equal terms. The sum over i is also trivial, as all the terms entering the summation are identical. Therefore we arrive at

$$E_2 = \frac{N(N-1)}{2}\eta\int d\vec{r}|\phi(\vec{r})|^4. \tag{23}$$

If we consider a large number of particles $N \gg 1$, then we can approach $N-1 \simeq N$. In this case, the energy functional $E = E_1 + E_2$ becomes

$$E[\phi,\phi^*] = N\int d\vec{r}\phi^*(\vec{r})\left(-\frac{\hbar^2}{2m}\nabla^2 + V_{ext}(\vec{r})\right)\phi(\vec{r}) + \frac{N^2}{2}\eta\int d\vec{r}|\phi(\vec{r})|^4. \tag{24}$$

Since the above energy functional depends on the single particle state ϕ, it is more convenient to introduce the energy per particle $E_P \equiv E/N$. Moreover, we can account for the normalisation condition by means of a Lagrange multiplier λ

$$\delta[E/N - \lambda(\langle\phi|\phi\rangle - 1)] = 0. \tag{25}$$

Thus, the functional we finally have to minimise is

$$E'_P[\phi,\phi^*] = \int d\vec{r}\phi^*(\vec{r})\left(-\frac{\hbar^2}{2m}\nabla^2 + V_{ext}(\vec{r})\right)\phi(\vec{r}) + \frac{N}{2}\eta\int d\vec{r}|\phi(\vec{r})|^4 - \lambda\int d\vec{r}|\phi(\vec{r})|^2. \tag{26}$$

Calculating $\delta E'_P$, one obtains

$$\delta E'_P = \int d\vec{r}\delta\phi^*(\vec{r}) \left[-\frac{\hbar^2}{2m}\nabla^2 + V_{ext}(\vec{r}) \right] \phi(\vec{r}) + N\eta \int d\vec{r}\delta\phi^*(\vec{r})|\phi(\vec{r})|^2\phi(\vec{r})$$
$$-\lambda \int d\vec{r}\delta\phi^*(\vec{r})\phi(\vec{r}) + C.C. \tag{27}$$

where the factor 1/2 has disappeared in the third term because there are two equal factors $\phi^*(\vec{r})$ that can vary in the integral.

As can be seen, $\delta\phi$ and $\delta\phi^*$ enter the above expression of $\delta E'_P$ as two independent variations. Thus, we can vary only $\phi^*(\vec{r})$, keeping $\phi(\vec{r})$ unaltered ($\delta\phi(\vec{r}) = 0$). In doing so, we obtain

$$\int d\vec{r}\delta\phi^*(\vec{r}) \left[-\frac{\hbar^2}{2m}\nabla^2 + V_{ext}(\vec{r}) + N\eta|\phi(\vec{r})|^2 - \lambda \right] \phi(\vec{r}) = 0. \tag{28}$$

This last equation must be satisfied for any arbitrary variation $\delta\phi^*(\vec{r})$. Using the fundamental lemma of the calculus of variations, the solution of Eq. (28) is given by

$$\left[-\frac{\hbar^2}{2m}\nabla^2 + V_{ext}(\vec{r}) + N\eta|\phi(\vec{r})|^2 \right] \phi(\vec{r}) = \lambda\phi(\vec{r}). \tag{29}$$

Interpretation of the Lagrange multiplier λ

Multiplying Eq. (29) from the left by $\phi^*(\vec{r})$ and integrating over $d\vec{r}$, one obtains

$$\lambda = \int d\vec{r} \left[-\frac{\hbar^2}{2m}\phi^*(\vec{r})\nabla^2\phi(\vec{r}) + \phi^*(\vec{r})V_{ext}(\vec{r})\phi(\vec{r}) + N\eta|\phi(\vec{r})|^4 \right]. \tag{30}$$

Next, we calculate $\partial E/\partial N$ to compare with the previous result. From Eq. (24) we have

$$\frac{\partial E}{\partial N} = \int d\vec{r}\phi^*(\vec{r}) \left(-\frac{\hbar^2}{2m}\nabla^2 + V_{ext}(\vec{r}) \right) \phi(\vec{r}) + N\eta \int d\vec{r}|\phi(\vec{r})|^4. \tag{31}$$

Hence, comparing Eqs. (30) and (31), one finds that $\lambda = \partial E/\partial N$. In words, λ is the variation of the total average energy when we add a particle to the system. This process is done at constant entropy S (keeping $T = 0$), so that $\partial E/\partial N$ becomes the chemical potential μ. Substituting $\lambda = \mu$ in Eq. (29), we finally arrive at the stationary Gross–Pitaevskii equation

$$\left[-\frac{\hbar^2}{2m}\nabla^2 + V_{ext}(\vec{r}) + N\eta|\phi(\vec{r})|^2 \right] \phi(\vec{r}) = \mu\phi(\vec{r}). \tag{32}$$

4.2 Time dependent Gross–Pitaevskii equation

In what follows, we derive the time-dependent Gross-Pitaevskii equation by making use of the variational principle of Dirac–Frenkel

$$\delta\langle\psi|\left(H-i\hbar\frac{\partial}{\partial t}\right)|\psi\rangle=0. \tag{33}$$

Dividing the above equation by the number of particles N, we have

$$\delta(E/N)-\delta\left[\frac{i\hbar}{N}\langle\psi|\frac{\partial}{\partial t}|\psi\rangle\right]=0, \tag{34}$$

where the first term has been calculated in the previous subsection. We will therefore focus on the calculation of the second term:

$$\begin{aligned}\langle\psi|\frac{\partial}{\partial t}|\psi\rangle &= \int d\vec{r}_1...d\vec{r}_N\psi^*(\vec{r}_1,...,\vec{r}_N)\frac{\partial}{\partial t}\psi(\vec{r}_1,...,\vec{r}_N)\\ &= \int d\vec{r}_1...d\vec{r}_N\phi^*(\vec{r}_1)...\phi^*(\vec{r}_N)\frac{\partial}{\partial t}[\phi(\vec{r}_1)...\phi(\vec{r}_N)]\\ &= \int d\vec{r}_1...d\vec{r}_N\phi^*(\vec{r}_1)\frac{\partial\phi(\vec{r}_1)}{\partial t}|\phi(\vec{r}_2)|^2...|\phi(\vec{r}_N)|^2+\\ &+\int d\vec{r}_1...d\vec{r}_N|\phi(\vec{r}_1)|^2\phi^*(\vec{r}_2)\frac{\partial\phi(\vec{r}_2)}{\partial t}|\phi(\vec{r}_3)|^2...|\phi(\vec{r}_N)|^2+...\\ &= \int d\vec{r}_1\phi^*(\vec{r}_1)\frac{\partial\phi(\vec{r}_1)}{\partial t}+...+\int d\vec{r}_N\phi^*(\vec{r}_N)\frac{\partial\phi(\vec{r}_N)}{\partial t}\,,\end{aligned} \tag{35}$$

where use has been made of the normalisation condition. Due to the fact that all the integrals in the last equality are identical, we finally obtain

$$\langle\psi|\frac{\partial}{\partial t}|\psi\rangle=N\int d\vec{r}\phi^*(\vec{r})\frac{\partial\phi(\vec{r})}{\partial t}\,. \tag{36}$$

Substituting Eqs. (27) (with $\lambda\equiv 0$) and (36) into Eq. (34), one arrives at

$$\int d\vec{r}\delta\phi^*(\vec{r})\left[-\frac{\hbar^2}{2m}\nabla^2+V_{ext}(\vec{r})+N\eta|\phi(\vec{r})|^2\right]\phi(\vec{r})-i\hbar\int d\vec{r}\delta\phi^*(\vec{r})\frac{\partial\phi(\vec{r})}{\partial t}+C.C.=0 \tag{37}$$

From the above equation, taking into account the linear independence of the $\delta\phi$ and $\delta\phi^*$ variations, it readily follows the time-dependent Gross–Pitaevskii equation

$$\left(-\frac{\hbar^2}{2m}\nabla^2+V_{ext}(\vec{r})+N\eta|\phi(\vec{r},t)|^2\right)\phi(\vec{r},t)=i\hbar\frac{\partial\phi(\vec{r},t)}{\partial t}\,. \tag{38}$$

5 Madelung equations

Las ecuaciones de Madelung se obtienen generalmente a partir de la ecuación de Schrödinger y son una formulación equivalente de ésta, escritas en términos de variables hidrodinámicas. En esta sección se utiliza el mismo procedimiento pero se parte de la ecuación de Gross–Pitaevskii, extrayendo así unas ecuaciones muy similares para los condensados de Bose–Einstein.

The Madelung equations, or quantum hydrodynamic equations, are an alternative and equivalent formulation of the Schrödinger equation written in terms of hydrodynamic variables. In what follows, we will derive the Madelung equations for the Gross–Pitaevskii equation, which only differs from the Schrödinger equation by the presence of the nonlinear term $N\eta|\phi(\vec{r},t)|^2\phi(\vec{r},t)$.

For our purposes, it is most convenient to introduce a new wave function φ, defined as

$$\varphi(\vec{r},t) = \sqrt{N}\phi(\vec{r},t). \tag{39}$$

This wave function is normalised to the number of particles N

$$\int d\vec{r}|\varphi(\vec{r},t)|^2 = N, \tag{40}$$

and its probability density coincides with the particle density

$$\rho(\vec{r},t) = |\varphi(\vec{r},t)|^2. \tag{41}$$

In terms of $\varphi(\vec{r},t)$, the GPE (38) takes the form

$$\frac{-\hbar^2}{2m}\nabla^2\varphi(\vec{r},t) + V_{ext}(\vec{r})\varphi(\vec{r},t) + \eta|\varphi(\vec{r},t)|^2\varphi(\vec{r},t) = i\hbar\frac{\partial\varphi(\vec{r},t)}{\partial t}\,. \tag{42}$$

To derive the Madelung equations, we rewrite the wave function φ in the so-called Madelung form ("de Broglie ansatz")

$$\varphi(\vec{r},t) = \sqrt{\rho(\vec{r},t)}\, e^{iS(\vec{r},t)/\hbar}, \tag{43}$$

where S has units of action and ρ is the particle density given by Eq. (41). Since, both $\rho(\vec{r},t)$ and $S(\vec{r},t)$ are real-valued functions, the above expression can be considered as the polar form of the wave function.

Substituting Eq. (43) in Eq. (42) and taking into account that

$$\frac{\partial}{\partial t}(\sqrt{\rho}e^{iS/\hbar}) = \frac{1}{2\sqrt{\rho}}\frac{\partial\rho}{\partial t}e^{iS/\hbar} + \sqrt{\rho}\frac{i}{\hbar}e^{iS/\hbar}\frac{\partial S}{\partial t}, \tag{44}$$

$$\nabla(\sqrt{\rho}e^{iS/\hbar}) = (\nabla\sqrt{\rho})e^{iS/\hbar} + \sqrt{\rho}\frac{i}{\hbar}e^{iS/\hbar}\nabla S, \tag{45}$$

$$\nabla^2(\sqrt{\rho}e^{iS/\hbar}) = \left[\nabla^2\sqrt{\rho} + 2\frac{i}{\hbar}\nabla\sqrt{\rho}\nabla S - \frac{\sqrt{\rho}}{\hbar^2}(\nabla S)^2 + \frac{i}{\hbar}\sqrt{\rho}\nabla^2 S\right] e^{iS/\hbar}, \tag{46}$$

we obtain

$$\left[\frac{-\hbar^2}{2m}\nabla^2\sqrt{\rho} - \frac{i\hbar}{m}\nabla\sqrt{\rho}\,\nabla S + \frac{\sqrt{\rho}}{2m}(\nabla S)^2 - \frac{i\hbar}{2m}\sqrt{\rho}\,\nabla^2 S\right] e^{iS/\hbar} + [V_{ext} + \eta\rho]\sqrt{\rho}e^{iS/\hbar} =$$

$$= \frac{i\hbar}{2\sqrt{\rho}}\frac{\partial\rho}{\partial t}e^{iS/\hbar} - \sqrt{\rho}\,\frac{\partial S}{\partial t}e^{iS/\hbar}. \tag{47}$$

Dividing Eq. (47) by $\varphi = \sqrt{\rho}e^{iS/\hbar}$, we arrive at

$$\frac{-\hbar^2}{2m}\frac{\nabla^2\sqrt{\rho}}{\sqrt{\rho}} - \frac{i\hbar}{m}\frac{\nabla\sqrt{\rho}\,\nabla S}{\sqrt{\rho}} + \frac{(\nabla S)^2}{2m} - \frac{i\hbar}{2m}\nabla^2 S + V_{ext} + \eta\rho = \frac{i\hbar}{2\rho}\frac{\partial\rho}{\partial t} - \frac{\partial S}{\partial t}. \tag{48}$$

To extract the two Madelung equations, we separate the real and imaginary parts from the above expression

Imaginary part:

$$\frac{\hbar}{m}\frac{\nabla\sqrt{\rho}}{\sqrt{\rho}}\nabla S + \frac{\hbar}{2m}\nabla^2 S + \frac{\hbar}{2\rho}\frac{\partial\rho}{\partial t} = 0. \tag{49}$$

We define the flux velocity as

$$\vec{v}(\vec{r},t) = \frac{\nabla S(\vec{r},t)}{m}. \tag{50}$$

Hence, $\vec{v}(\vec{r},t)$ is irrotational

$$\nabla\times\vec{v} = \vec{0}. \tag{51}$$

Taking into account that

$$\nabla^2 S = \nabla(\nabla S) = m\nabla\vec{v}, \tag{52}$$

$$\nabla\sqrt{\rho} = \frac{1}{2\sqrt{\rho}}\nabla\rho, \tag{53}$$

Eq. (49) can be rewritten as

$$\frac{1}{2\rho}(\nabla\rho)\vec{v} + \frac{1}{2}\nabla\vec{v} + \frac{1}{2\rho}\frac{\partial\rho}{\partial t} = 0. \tag{54}$$

Multiplying by 2ρ

$$(\nabla\rho)\vec{v} + \rho\nabla\vec{v} + \frac{\partial\rho}{\partial t} = 0. \tag{55}$$

By using the properties of the nabla operator to group the first two terms, we reach the first Madelung equation (continuity equation)

$$\frac{\partial\rho}{\partial t} + \nabla(\rho\vec{v}) = 0. \tag{56}$$

This equation is analogous to the continuity equations of Fluid Dynamics or Electromagnetism, which express the mass and charge conservation, respectively. In this case, the equation (56) informs us that the probability of finding a particle in a certain volume V is conserved. The quantity $\rho\vec{v}$ is the so-called flux density.

Real part:

$$\frac{-\hbar^2}{2m}\frac{\nabla^2\sqrt{\rho}}{\sqrt{\rho}} + \frac{(\nabla S)^2}{2m} + V_{ext} + \eta\rho = -\frac{\partial S}{\partial t}. \tag{57}$$

The first term

$$Q = \frac{-\hbar^2}{2m}\frac{\nabla^2\sqrt{\rho}}{\sqrt{\rho}}, \tag{58}$$

is known by the name of Quantum potential or Quantum pressure. In this way, the equation (57) can be written as follows:

$$\frac{(\nabla S)^2}{2m} + V_{ext} + Q + \eta\rho = -\frac{\partial S}{\partial t}. \tag{59}$$

The term $\eta\rho$ comes from the nonlinear term $\eta|\varphi|^2\varphi$ of the GPE (42). If this term were not present, that is if we started from the Schrödinger equation instead of the GPE, then Eq. (59) would be the Quantum Hamilton–Jacobi equation. This is a very important equation since it represents a bridge between quantum and classical mechanics. To go from the former to the latter, one would take the limit $\hbar \to 0$, eliminating thereby the quantum potential and obtaining directly the classical Hamilton–Jacobi equation, which is an alternative formulation of Classical Mechanics.

Applying the nabla operator on both sides of Eq. (59) and taking into account Eq. (50), one obtains

$$-\frac{1}{2}m\nabla\vec{v}^2 - \nabla V_{ext} - \nabla Q - \nabla(\eta\rho) = m\frac{\partial\vec{v}}{\partial t}. \tag{60}$$

Using the following property of the nabla operator for irrotational vector fields:

$$\nabla(\vec{v}\vec{v}) = 2(\vec{v}\,\nabla)\vec{v}, \tag{61}$$

Eq. (60) finally takes the form

$$m\left[\frac{\partial\vec{v}}{\partial t}+(\vec{v}\,\nabla)\vec{v}\right]=-\nabla V_{ext}-\nabla Q-\nabla(\eta\rho). \tag{62}$$

This is the second Madelung equation we were looking for. It can be shown that the pressure of a BEC is given by $P=\frac{1}{2}\eta\rho^2$. As a result, $\nabla P=\rho\nabla(\eta\rho)$ and the last term of Eq. (62) becomes $\nabla(\eta\rho)=(\nabla P)/\rho$. With this, neglecting the contribution from the quantum pressure, Eq. (62) coincides with the Euler equation of Fluid Dynamics.

6 Stationary self-graviting Bose–Einstein condensates

Una vez extraídas las ecuaciones de Madelung imponemos en éstas que el condensado se encuentre en estado estacionario y únicamente sometido a la interacción gravitatoria. De esta manera derivaremos una ecuación de Helmholtz para la densidad de masa que se puede resolver de la misma forma que la ecuación de Schrödinger para una partícula libre. Al final de esta sección se obtiene una ecuación que describe la densidad de un condensado en las circunstancias impuestas.

Since our aim is to model dark matter as a BEC, in what follows we consider a stationary ($\vec{v}=\vec{0}$) self-graviting Bose–Einstein condensate. In this case, the external potential reads

$$V_{ext}(\vec{r})=V_g(\vec{r})=m\Phi(\vec{r}), \tag{63}$$

where the gravitational potential Φ satisfies the Poisson equation

$$\nabla^2\Phi=4\pi G\rho_m. \tag{64}$$

G is the gravitational constant and $\rho_m\equiv m\rho=m|\varphi(\vec{r},t)|^2$ is the mass density of the condensate.

An approximation commonly used in the study of Bose–Einstein condensates is the so-called Thomas–Fermi approximation. It essentially consists in taking the classical limit of the theory, considering negligible all the terms in higher powers of $\hbar$. The larger the number N of particles in the condensate, the better the Thomas–Fermi approximation. In particular, in the $N\to\infty$ limit this approximation becomes exact.

As is evident from Eq. (58), in our case the Thomas–Fermi approximation amounts to neglecting the contribution from the quantum pressure Q in Eq. (62)

$$0=\nabla V_g+\nabla(\eta\rho). \tag{65}$$

Applying the nabla operator to the above equation, using Eqs. (63) and (64) and substituting $\rho = \rho_m/m$, we get

$$0 = m(4\pi G\rho_m) + (\eta/m)\nabla^2\rho_m. \tag{66}$$

On the other hand, making use of the stationary condition $\vec{v} = \vec{0}$ in the first Madelung equation (56), we obtain

$$\frac{\partial\rho(\vec{r},t)}{\partial t} = 0, \tag{67}$$

which, taking into account that $\rho_m = m\rho$, implies

$$\rho_m(\vec{r},t) = \rho_m(\vec{r}). \tag{68}$$

Using this result in Eq. (66), one finds that the mass density $\rho_m(\vec{r})$ satisfies a Helmholtz equation

$$[\nabla^2 + k^2]\rho_m(\vec{r}) = 0, \tag{69}$$

with

$$k^2 = \frac{4\pi G m^2}{\eta}. \tag{70}$$

Expressing the Laplace operator ∇^2 in spherical coordinates, Eq. (69) reads

$$\left[\frac{1}{r^2}\frac{\partial}{\partial r}\left(r^2\frac{\partial}{\partial r}\right) + \frac{1}{r^2\sin\theta}\frac{\partial}{\partial\theta}\left(\sin\theta\frac{\partial}{\partial\theta}\right) + \frac{1}{r^2\sin^2\theta}\frac{\partial^2}{\partial\phi^2} + k^2\right]\rho_m(\vec{r}) = 0. \tag{71}$$

In quantum mechanics, the square of the angular momentum operator $\vec{L}$ in spherical coordinates is given by

$$\vec{L}^2 = -\hbar^2\left[\frac{1}{\sin\theta}\frac{\partial}{\partial\theta}\left(\sin\theta\frac{\partial}{\partial\theta}\right) + \frac{1}{\sin^2\theta}\frac{\partial^2}{\partial\phi^2}\right]. \tag{72}$$

Then, we can rewrite Eq. (71) as

$$\left[\frac{1}{r^2}\frac{\partial}{\partial r}\left(r^2\frac{\partial}{\partial r}\right) - \frac{\vec{L}^2}{\hbar^2 r^2} + k^2\right]\rho_m(\vec{r}) = 0. \tag{73}$$

Multiplying by the factor $-\hbar^2/2m$, we obtain an eigenvalue equation that is formally analogous to the Schrödinger equation for a free particle (or, in other words, a particle in a zero central potential $V(r) = 0$)

$$\left[\frac{-\hbar^2}{2m}\frac{1}{r^2}\frac{\partial}{\partial r}\left(r^2\frac{\partial}{\partial r}\right) + \frac{\vec{L}^2}{2mr^2}\right]\rho_m(\vec{r}) = \frac{\hbar^2k^2}{2m}\rho_m(\vec{r}). \tag{74}$$

However, despite the formal analogy it is important to bear in mind that Eq. (74) involves the mass density $\rho_m(\vec{r}) \equiv m|\varphi(\vec{r})|^2$ instead of the particle wave function.

For the sake of simplifying the notation, in what follows we drop the sub-index m in the expression of the mass density, $\rho_m(\vec{r}) \equiv \rho(\vec{r})$.

As the operators L_x, L_y, L_z and $\vec{L}^2$ do not act on the radial variable, if we name J the operator in brackets of the above equation, we have

$$[J, \vec{L}] = [J, \vec{L}^2] = 0. \tag{75}$$

Since also $[\vec{L}^2, \vec{L}] = 0$, we can take as usual the set of commuting operators $\{J, \vec{L}^2, L_z\}$ in order to find solutions of Eq. (74) that are simultaneous eigenfunctions of $\vec{L}^2$ and L_z.

As is well known, the eigenfunctions of the orbital angular momentum are the spherical harmonics $Y_{lm}(\theta, \phi)$

$$\vec{L}^2 Y_{lm}(\theta, \phi) = l(l+1)\hbar^2 Y_{lm}(\theta, \phi), \tag{76}$$

$$L_z Y_{lm}(\theta, \phi) = m\hbar Y_{lm}(\theta, \phi). \tag{77}$$

Taking into account Eqs. (76) and (77), we search for solutions of Eq. (74) using separation of variables

$$\rho_{klm}(\vec{r}) = R_{klm}(r) Y_{lm}(\theta, \phi). \tag{78}$$

Substituting in Eq. (74), one finds that the unknown radial part must satisfy

$$\left[\frac{-\hbar^2}{2m}\frac{1}{r^2}\frac{d}{dr}\left(r^2\frac{d}{dr}\right) + \frac{l(l+1)\hbar^2}{2mr^2}\right] R_{kl}(r) = \frac{\hbar^2 k^2}{2m} R_{kl}(r), \tag{79}$$

where we have dropped the sub-index m from the radial function because Eq. (79) does not depend on this quantum number.

Recalling that $|m| \leq l$, we have $2l+1$ eigenfunctions $\rho_{klm}(\vec{r})$ for a certain pair (k, l).

Equation (79) can be rewritten as

$$\left[\frac{-\hbar^2}{2m}\frac{d^2}{dr^2} - \frac{\hbar^2}{mr}\frac{d}{dr} + \frac{l(l+1)\hbar^2}{2mr^2}\right] R_{kl}(r) = \frac{\hbar^2 k^2}{2m} R_{kl}(r). \tag{80}$$

Multiplying both sides by r and denoting the centrifugal term $l(l+1)\hbar^2/2mr^2$ by $V_{\text{eff}}(r)$, the above equation becomes

$$\frac{-\hbar^2}{2m}\left[r R''_{kl}(r) + 2R'_{kl}(r)\right] + V_{\text{eff}}(r)\, r R_{kl}(r) = \frac{\hbar^2 k^2}{2m}\, r R_{kl}(r). \tag{81}$$

Making the change of variable $u = rR$, Eq. (81) can be rewritten as

$$\frac{-\hbar^2}{2m} u''_{kl}(r) + V_{\text{eff}}(r)\, u_{kl}(r) = \frac{\hbar^2 k^2}{2m} u_{kl}(r). \tag{82}$$

The solutions $u_{kl}(r)$ are only defined for $r \geq 0$. Since the radial functions $R_{kl}(r) = u_{kl}(r)/r$ must remain finite at the origin, $u_{kl}(r)$ has to satisfy the boundary condition.

$$u_{kl}(0) = 0. \tag{83}$$

The centrifugal term $V_{\text{eff}}(r)$ has its origin in the Laplacian operator and, thus, it also contributes to the system Hamiltonian (10) through the kinetic energy. Since this term is always positive, the greater the angular momentum, the greater the energy of the system. Although higher energy solutions with any $l > 0$ are possible, in this work we will focus in the lowest energy ($l = 0$) solutions (with no angular momentum). In this case, Eq. (82), reduces to

$$\left[\frac{d^2}{dr^2} + k^2\right] u_{k0}(r) = 0. \tag{84}$$

This is a second-order linear homogeneous differential equation whose particular solution satisfying the boundary condition (83) is

$$u_{k0}(r) = A \sin(kr). \tag{85}$$

Taking into account that $Y_{00}(\theta, \phi) = 1/\sqrt{4\pi}$, after substituting $R_{k0}(r) = u_{k0}(r)/r$ in the expression (78) for the mass density $\rho_{k00}(\vec{r}) \equiv \rho(r)$, one obtains

$$\rho(r) = \rho_c \frac{\sin(kr)}{kr}, \tag{86}$$

where $\rho_c = \lim_{r\to 0} \rho(r)$ is the central mass density of the self-graviting condensate.

7 Dark matter as Bose–Einstein condensates

Teniendo el perfil de densidad para un condensado estacionario atrapado gravitacionalmente, podemos utilizarlo para modelar los halos de materia oscura de las galaxias. Aquí se extraen las características más importantes de estos halos, como la masa o la curva de velocidades de rotación, con el objetivo de poder comparar este modelo con el modelo estándar (CDM).

Once we have obtained the mass density $\rho(r)$, we can derive other properties of the dark matter halo such as its radius, mass as a function of r, total mass, or the velocity profile of the rotation curves.

The halo radius R (radius of the condensate) follows from the condition that the mass density vanishes at R, $\rho(R) = 0$, which from Eq. (86) leads to $kR = n\pi$ with $n \in \mathbb{N}$. However, since $\rho(r)$ may not take negative values, only the first zero ($kR = \pi$) is meaningful and $\rho(r)$ must vanish for $r \geq R$. Recalling the expressions of k and η given, respectively, by Eqs. (70) and (21), we obtain

$$R = \frac{\pi}{k} = \pi\sqrt{\frac{\hbar^2 a_s}{Gm^3}}. \tag{87}$$

Next, we look for a function $m(r)$ that for each r returns the mass inside a sphere of radius r. Assuming spherical symmetry, the element of mass in an element of volume, $dm = \rho dV$, can be expressed as

$$dm = 4\pi\rho(r)r^2 dr, \tag{88}$$

and integrating

$$m(r) = 4\pi\int_0^r \rho(r)r^2 dr = \frac{4\pi\rho_c}{k}\int_0^r \sin(kr)r dr. \tag{89}$$

Denoting the last integral by I and integrating by parts, we get

$$I = \left[-\frac{r\cos(kr)}{k}\right]_0^r + \int_0^r \frac{\cos(kr)}{k}dr = -\frac{r\cos(kr)}{k} + \frac{\sin(kr)}{k^2} = \frac{\sin(kr)}{k^2}[1 - kr\cot(kr)]. \tag{90}$$

Using this result in Eq. (89) and taking into account Eq. (86), we get the following expression for the mass bounded by a sphere of radius r:

$$m(r) = \frac{4\pi}{k^2}\, r\rho(r)[1 - kr\cot(kr)]. \tag{91}$$

The halo mass M is readily obtained from the above equation

$$M = m(R) = \frac{4\pi}{k^3}\rho_c \sin(kR)[1 - kR\cot(kR)] = \frac{4\pi R^3\rho_c}{\pi^3}[\sin\pi - \pi\cos(\pi)], \tag{92}$$

where we have used Eq. (86) in the second equality and the relation $kR = \pi$ in the third one. Substituting Eq. (87), we finally arrive at

$$M = \frac{4R^3\rho_c}{\pi} = 4\pi^2\rho_c\left(\frac{\hbar^2 a_s}{Gm^3}\right)^{3/2}. \tag{93}$$

Supposing a spherical volume of radius R one can extract the average density of the condensate

$$\langle\rho\rangle = \frac{M}{V} = \frac{4R^3\rho_c/\pi}{(4/3)\pi R^3} = \frac{3\rho_c}{\pi^2}. \tag{94}$$

However, the most important aspect of a dark matter model is the velocity profile it generates. Equation (2) in Sec. 2 models the tangential velocity of a test particle moving inside the dark halo. Introducing in this equation the expression (91) for $m(r)$ obtained in the context of the above BEC dark matter model, we get

$$v^2(r) = \frac{Gm(r)}{r} = \frac{4\pi G\rho(r)}{k^2}[1 - kr\cot(kr)] = \frac{4G\rho_c R^2}{\pi}\left[\frac{\sin(\pi r/R)}{\pi r/R} - \cos\left(\frac{\pi r}{R}\right)\right]. \tag{95}$$

As a function of the total mass, we can rewrite Eq. (95) in the form

$$v^2(r) = \frac{GM}{R}\left[\frac{\sin(\pi r/R)}{\pi r/R} - \cos\left(\frac{\pi r}{R}\right)\right]. \tag{96}$$

For $r > R$ the rotation curves follow the standard Keplerian law.

8 Numerical results

En esta sección se estudian los resultados para la curva de densidad y el perfil de velocidades de rotación dentro del marco de este modelo, y se comparan con los resultados del modelo CDM y con los resultados observacionales para siete galaxias de la base de datos SPARC.

The main purpose of this work is to compare the cold dark matter model with our model based on Bose–Einstein condensates, as done previously in Refs. [5] and [6]. To this end, using the results of Ref. [7], we have chosen a number of galaxies of the SPARC survey [8] which are principally composed of dark matter and have high resolution experimental rotation curves.

As already said in the introduction, in the CDM model the mass density is described by the Navarro–Frenk–White (NFW) profile

$$\rho_{NFW}(r) = \frac{\rho_s}{(r/r_s)(1 + r/r_s)^2}. \tag{97}$$

For this density profile the rotational velocity is given by

$$v_{NFW}(r) = \sqrt{4\pi G\rho_s r_s^3}\,\sqrt{\frac{1}{r}\left[\ln\left(1 + \frac{r}{r_s}\right) - \frac{(r/r_s)}{1 + r/r_s}\right]}. \tag{98}$$

To compare the rotation curves of both models we have fitted their velocity profiles [Eqs. (95) and (98)] to observational data, obtaining the optimal parameters ρ_s and

r_s for the NFW model and ρ_c and R for the BEC model (see Appendix A). The SPARC galaxy database provides the observational velocities (V) at different radii, the contribution of the gas to this velocity (V_{gas}) and the contributions of the bulge (V_{bul}) and the disk (V_{disk}). According to the instructions of Ref. [8], the dark matter contribution is given by

$$V_{DM} = \sqrt{V^2 - |V_{gas}|V_{gas} - \Upsilon_{disk}|V_{disk}|V_{disk}} \,, \tag{99}$$

where we have taken into account that $V_{bul} = 0$ in all the galaxies that we have used. Υ_{disk} is the stellar mass-to-light ratio of the disk component, since the velocity V_{disk} of the stars was calculated from their luminosity. We have used $\Upsilon_{disk} = 0.47$ according to the results of Ref. [9].

In Eq. (99) the absolute values are needed because sometimes the gas contribution to the velocity is negative. This is due to the fact that in the innermost regions of the halo it is possible to have a gas distribution which produces a stronger gravitational force from the outer regions of the gas than from the inner ones (a relative mass defect) [8].

Figure 5 shows the dark matter contribution to the velocities obtained from Eq. (99) (observational data) along with the fits of the BEC and the NFW models for a number of galaxies of the SPARC database. As can be seen, for the majority of these galaxies the BEC model fits better to the observational rotation curves.

From the fitting parameters of both models we can also infer the density profiles of the corresponding halos.

An aspect one can observe from Eq. (97) is that the NFW profile, based on numerical simulations of the CDM model, presents a singularity or cusp at the centre of the galaxies ($r \to 0$). As a result, the NFW mass distribution decreases abruptly around the cusp. This problem (cusp-core problem) is avoided by the BEC model, which produces a finite central density ρ_c. This difference is reflected in the fact that the mass distribution of the gravitationally bounded condensate decreases slowly as a function of r with a major part of the matter concentrated in a core-like region. The predictions of both models for the dark matter density profiles of the different galaxies are shown in Figs. 6 and 7.

Another difference between these models is that, even though for large r the NFW profile tends more rapidly to zero, its behaviour is asymptotic and therefore the DM halo described by this model has not physical limits. In contrast, the BEC density curve tends rigorously to zero on a surface well defined by the radius R. In this way, Bose–Einstein condensates predict a flatter central dark matter distribution than cosmological simulations, resulting in dark matter halos more similar to those found observationally.

We can use the obtained value of R as an additional guarantee that we have achieved

a good fit, because the radius R is interpreted as the point where the rotation curve starts to decline and it can be extracted from observations. Comparing these two values for the different galaxies we have a reinforcement of the viability of the BEC dark matter model.

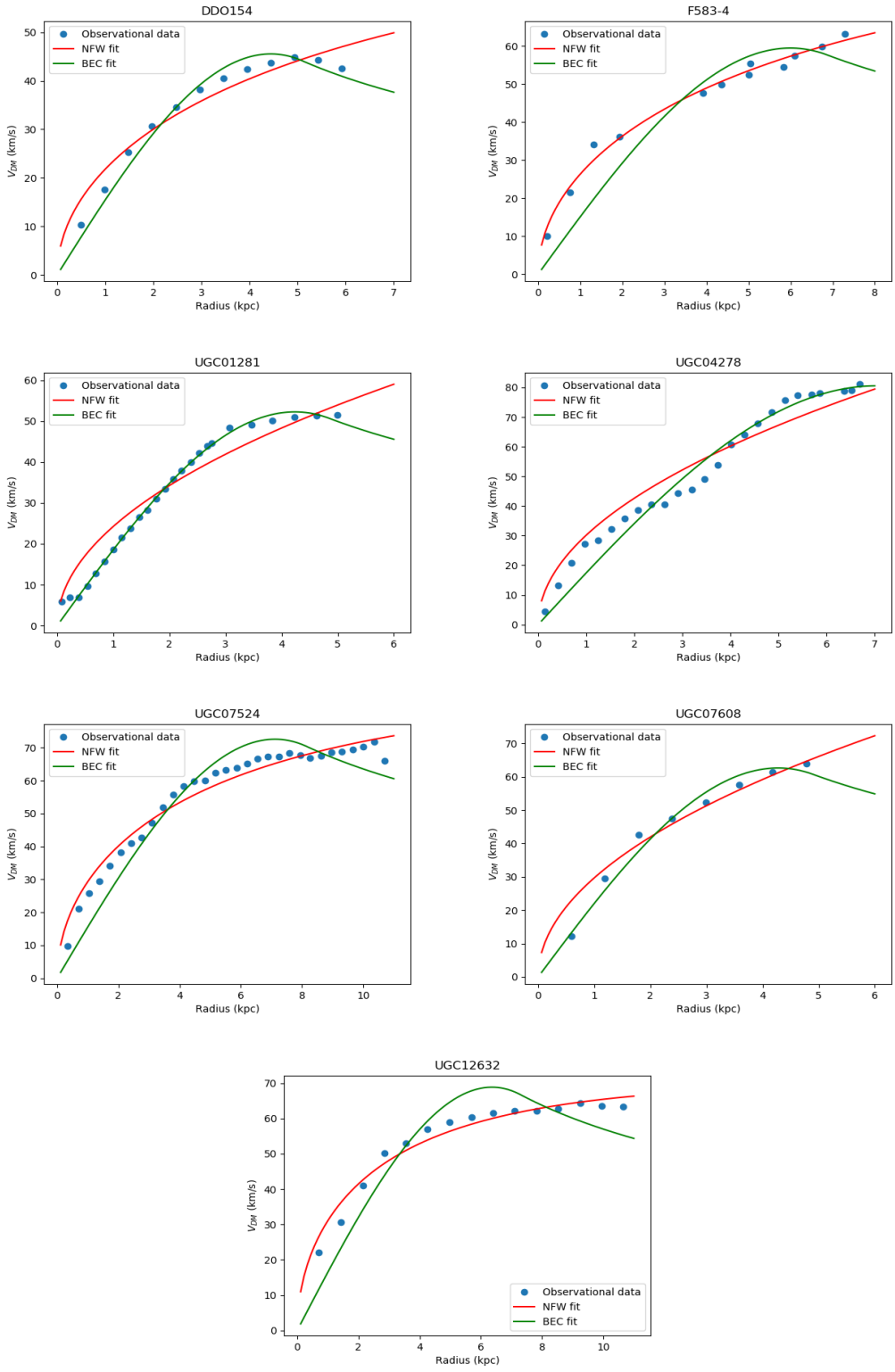

Figure 5: Fits to the dark matter contribution to rotational velocities for the BEC model (green line) and the NFW profile (red line) for seven galaxies. Data extracted from SPARC [8].

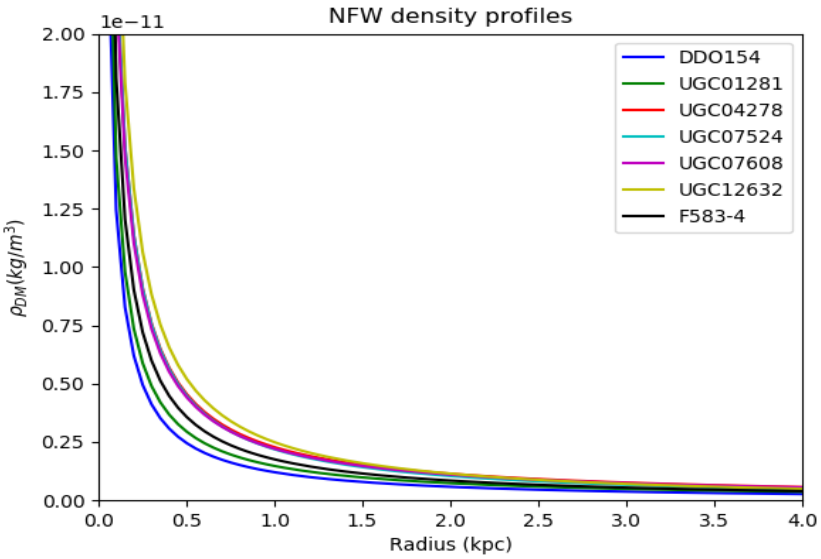

Figure 6: NFW dark matter density profiles for the galaxies considered in Fig. 5.

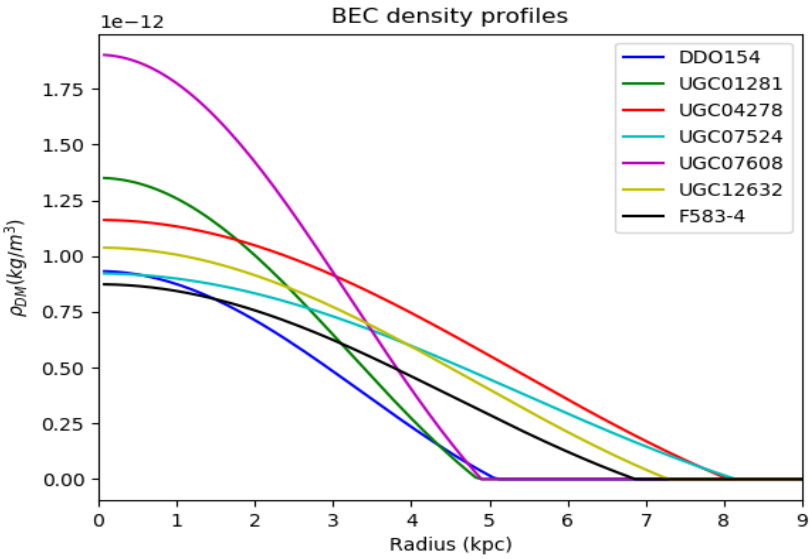

Figure 7: BEC dark matter density profiles for the galaxies considered in Fig. 5.

9 Conclusions

En esta sección final se evalúan los problemas de este modelo simplificado y se contemplan modelos de condensados más complejos.

We have derived in detail the Gross–Pitaevskii equation describing a Bose–Einstein condensate and have used this equation to model dark matter halos as self-graviting Bose–Einstein condensates. Using the Thomas–Fermi approximation we have analytically solved the relevant equations and have obtained the physical properties of the halos: radii, masses, density profiles and circular rotation curves. Then, we have developed a numerical code (Appendix A) and have compared the predictions from this BEC model with those from the standard ΛCDM model for a number of galaxies extracted from the SPARC database [8]. The obtained results indicate that the BEC model can fit the observational data very well and at the same time it could solve the core-cusp problem. However, there are some caveats we will discuss in what follows.

From the results of Sec. 7, it can be seen that all the halo properties (mass, density, rotation velocity) depend only on two independent parameters: the central density ρ_c and the radius R. In turn, R depends on the individual particle mass m and the s-wave scattering length a_s through Eq. (87). The point is that a_s characterises the intensity of the particle-particle interaction and thus, it is an intrinsic property of each particle type. Changing a_s or m is equivalent to changing the particle type. Therefore, the values for the mass m and for the s-wave scattering length a_s should be the same for every halo. This would imply that all the halos would have the same radius R. In the previous section, however, we used different values of R to fit the different galaxies. In fact, the model presented in this work should be considered as a first approximation to the problem. Recent publications based on a more complete description involving numerical simulations highlight the fact that galaxy halos are actually made up of subhalos. In this scenario, the theoretical equations derived in the present work would only be valid for the central subhalo and a more elaborate treatment would require intensive numerical calculations.

As a natural continuation of this work, we propose to incorporate the contributions of ordinary matter and to recalculate the density profiles and the rotation curves for this general case. On the other hand, it would also be interesting to analyze the regime in which the interactions between particles are negligible. Under these circumstances, the Gross–Pitaevskii–Poisson equation reduces to a Schrödinger–Poisson equation. In this regime, which like the Thomas–Fermi regime is analytically solvable, the gravitational interaction is fully compensated by the quantum pressure.

Although the BEC model presented in this work is only a first approximation, it already reflects the potential of this kind of approaches based on Bose–Einstein condensates in the solution of the dark matter problem.

Appendix A Numerical code

```
import pylab as py
import numpy as np
from scipy.optimize import curve_fit
G = 6.674e-11       #SI
fc_R = 3.086e16     #Conversion factor from kpc to km
fc_rho = 1e12       #Conversion factor from g/cm^3 to kg/km^3
fc_G = 1e-9         #Conversion factor from m^3/kg.s^2 to km^3/kg.s^2
gamma=0.47


g1 = np.genfromtxt('DDO154_rotmod.txt', delimiter='\t', dtype=float)

radios_1 = np.array([])
vel_obs_1 = np.array([])
vel_gas_1 = np.array([])
vel_disk_1 = np.array([])
errV_1 = np.array([])


for line in np.arange(0, len(g1)):
    rad = g1[line][0]
    v_obs = g1[line][1]
    errv_obs = g1[line][2]
    v_gas = g1[line][3]
    v_disk = g1[line][4]

    radios_1 = np.append(radios_1, rad)
    vel_obs_1 = np.append(vel_obs_1, v_obs)
    vel_gas_1 = np.append(vel_gas_1, v_gas)
    vel_disk_1 = np.append(vel_disk_1, v_disk)
    errV_1 = np.append(errV_1, errv_obs)



vel_DM_1 = np.sqrt(vel_obs_1**2 - abs(vel_gas_1)*vel_gas_1 - gamma*
abs(vel_disk_1)*vel_disk_1)
err_VDM_1 = (vel_obs_1/vel_DM_1)*errV_1
```

```
def model_NFW(r, a, b):
    return np.sqrt(4*np.pi*G*fc_G*a*(b*fc_R)**3)*np.sqrt((1/(r*fc_R))*
    (np.log(1+r/b)-(r/b)/(1+r/b)) )


popt_1, pcov_1 = curve_fit(model_NFW, radios_1, vel_DM_1)



def model_BEC(r, p, R):
    return np.piecewise( r, [r<R, r>=R], [lambda r: R*fc_R*
    np.sqrt((4*p*G*fc_G)/np.pi)*np.sqrt( np.sin(np.pi*r/R)/(np.pi*r/R)
    - np.cos(np.pi*r/R) ), lambda r: np.sqrt(4*G*fc_G*R*(R*fc_R)**2*p/
    (r*np.pi))] )


popt2_1, pcov2_1 = curve_fit(model_BEC, radios_1, vel_DM_1)



x_model = np.linspace(0, 7, 100)

py.figure()
py.plot(radios_1, vel_DM_1, 'bo')
py.plot(x_model, model_NFW(x_model, *popt_1), 'r-')
py.plot(x_model, model_BEC(x_model, *popt2_1), 'g-')
py.errorbar(radios_1, vel_DM_1, yerr = err_VDM_1, fmt = 'bo')
py.title('DDO154')
py.legend(('Observational data', 'NFW fit', 'BEC fit'))
py.xlabel('Radius (kpc)')
py.ylabel('$V_{DM}$ (km/s)')

py.savefig('DDO154.png')



k_1 = np.pi/popt2_1[1]

def densityBEC_1(r):
    return np.piecewise(r, [r<popt2_1[1], r>=popt2_1[1]], [lambda r:
    popt2_1[0]*np.sin(k_1*r)/(k_1*r), lambda r: 0])
```

```
def densityNFW_1(r):
    return popt_1[0]/((r/popt_1[1])*(1+r/popt_1[1]))


#We repeated the same procedure for each of the galaxies



rt = np.linspace(0, 15, 200)

py.figure()
py.plot(rt, densityBEC_1(rt), 'b-')
py.plot(rt, densityBEC_2(rt), 'g-')
py.plot(rt, densityBEC_3(rt), 'r-')
py.plot(rt, densityBEC_4(rt), 'c-')
py.plot(rt, densityBEC_5(rt), 'm-')
py.plot(rt, densityBEC_6(rt), 'y-')
py.plot(rt, densityBEC_7(rt), 'k-')
py.title('BEC density profiles')
py.xlim(0, 9)
py.ylabel(r'$\rho_{DM} (kg/m^3)$')
py.xlabel('Radius (kpc)')
py.legend(('DDO154', 'UGC01281', 'UGC04278', 'UGC07524', 'UGC07608',
'UGC12632', 'F583-4'))

py.savefig('densities_BEC.png')



rt2 = np.linspace(0, 10, 200)

py.figure()
py.plot(rt2, densityNFW_1(rt2), 'b-')
py.plot(rt2, densityNFW_2(rt2), 'g-')
py.plot(rt2, densityNFW_3(rt2), 'r-')
py.plot(rt2, densityNFW_4(rt2), 'c-')
py.plot(rt2, densityNFW_5(rt2), 'm-')
py.plot(rt2, densityNFW_6(rt2), 'y-')
py.plot(rt2, densityNFW_7(rt2), 'k-')
py.title('NFW density profiles')
py.ylim(0, 2e-11)
py.xlim(0, 4)
```

```
py.ylabel(r'$\rho_{DM} (kg/m^3)$')
py.xlabel('Radius (kpc)')
py.legend(('DDO154', 'UGC01281', 'UGC04278', 'UGC07524', 'UGC07608',
'UGC12632', 'F583-4'))

py.savefig('densities_NFW.png')
```

References

[1] Fabian Walter, Elias Brinks, WJG De Blok, Frank Bigiel, Robert C Kennicutt Jr, Michele D Thornley, and Adam Leroy. THINGS: The HI nearby galaxy survey. *The Astronomical Journal*, 136(6):2563, 2008.

[2] Gianfranco Bertone and Dan Hooper. History of dark matter. *Reviews of Modern Physics*, 90(4):045002, 2018.

[3] CJ Pethick and H Smith. *Bose–Einstein condensation in dilute gases*. Cambridge University Press, 2008. ISBN 9780521846516.

[4] Franco Dalfovo, Stefano Giorgini, Lev P Pitaevskii, and Sandro Stringari. Theory of Bose–Einstein condensation in trapped gases. *Reviews of Modern Physics*, 71(3):463, 1999.

[5] CG Boehmer and T Harko. Can dark matter be a Bose–Einstein condensate? *Journal of Cosmology and Astroparticle Physics*, 2007(06):025, 2007.

[6] T Harko. Bose–Einstein condensation of dark matter solves the core/cusp problem. *Journal of Cosmology and Astroparticle Physics*, 2011(05):022, 2011.

[7] A. Muñoz Mateo and V. Delgado. Article in preparation. 2020.

[8] Federico Lelli, Stacy S. McGaugh, and James M. Schombert. SPARC: Mass models for 175 disk galaxies with spitzer photometry and accurate rotation curves. *The Astronomical Journal*, 152(6):157, Nov 2016. ISSN 1538-3881. doi: 10.3847/0004-6256/152/6/157. URL `http://dx.doi.org/10.3847/0004-6256/152/6/157`.

[9] Stacy S McGaugh and James M Schombert. Color-mass-to-light-ratio relations for disk galaxies. *The Astronomical Journal*, 148(5):77, 2014.

[10] Andrew Pontzen and Fabio Governato. Cold dark matter heats up. *Nature*, 506(7487):171–178, 2014.

[11] Andreas Burkert. The structure of dark matter halos in dwarf galaxies. *The Astrophysical Journal Letters*, 447(1):L25, 1995.

[12] Jesus Rogel-Salazar. The Gross–Pitaevskii equation and Bose–Einstein condensates. *European Journal of Physics*, 34(2):247, 2013.

[13] Mikel Quintana Uriarte. *Mecánica Hamiltoniana. Ecuación de Hamilton–Jacobi. Ejemplos y aplicaciones* (final degree project). Universidad del País Vasco. 2013.

[14] Lev Pitaevskii and Sandro Stringari. *Bose–Einstein Condensation and superfluidity*. Oxford University Press, Great Clarendon Street, Oxford, OX2 6DP, United Kingdom, 2016. ISBN 9780198758884.

[15] Katherine Freese. Review of observational evidence for dark matter in the universe and in upcoming searches for dark stars. *EAS Publications Series*, 36: 113–126, 2009.

[16] Claude Cohen-Tannoudji. *Condensation de Bose–Einstein des gaz atomiques ultra froids; effets des interactions. Cours de physique atomique et moléculaire.* Collège de France, 1998-1999.

[17] P-O Löwdin and PK Mukherjee. Some comments on the time-dependent variation principle. *Chemical Physics Letters*, 14(1):1–7, 1972.

[18] Hans-Dieter Meyer. *Introduction to MCTDH (Lecture notes)*, chapter 2, appendix B. Universität Heidelberg, 2011.

[19] Timothy C Wallstrom. Inequivalence between the Schrödinger equation and the Madelung hydrodynamic equations. *Physical Review A*, 49(3):1613, 1994.

[20] Alberto Casas González. *La materia oscura*. RBA, Spain, 2015. ISBN 9788447383016.

[21] B.H. Bransden and Charles Joachain. *Quantum Mechanics*. Prentice Hall, 01 2000. ISBN 0582-35691-1.